# Short-term dynamics of a high energy embayed beach: Stanwell Park, NSW, Australia

Rémy Asselot[1,2]*, Robert W. Brander[1]

[1] School of Biological, Earth and Environmental Sciences, UNSW Sydney, Sydney, Australia
[2] Present address: Ifremer, University of Brest, CNRS, IRD, Laboratoire d'Océanographie Physique et Spatiale (LOPS), IUEM, 29280 Plouzané, France

* Corresponding author: remy.assel@gmail.com

## ABSTRACT

The three-dimensional variability of the subaerial beach is examined for Stanwell Park Beach, New South Wales (NSW), Australia. This embayed environment has previously been studied over long time scales (decades), but not over shorter time scales (days, weeks). Embayed beaches experience rotation events during which opposite accretion and erosion patterns are observed at the extremities of the beach. To analyse this phenomenon, the beach is mapped with 10 Real-Time Kinematic Global Positioning System (RTK-GPS) surveys collected from 10th February 2016 to 14th May 2016. This study aims to examine short-term changes (days, weeks) to the morphology of the subaerial beach of Stanwell Park Beach and any factors that may influence its behaviours. We show that a short-time beach rotation event occurs over one month, caused by a large eastern swell. However, swell with a southern direction generates rip current channels on the subaerial beach face. During this particular event, the amount of sediment transported is lower than during beach rotation events. Furthermore, Stanwell Park Beach has two lagoons that can open to discharge water accumulated in these lagoons. We show that during heavy rainfall, the lagoons open, transporting sediment in surf zone and thus causing erosion. This study provides a clear demonstration of the sensitivity of embayed beaches to short-term variability in wave climate.

**Descriptors:** Stanwell Park Beach, Embayed beach, Beach behave, Beach rotation, RTK-GPS.

## INTRODUCTION

Human attraction to the coastal environment is constantly increasing. Previous studies indicate that the colonisation of the oceans is now perceptible and the density of urban areas reflects the development in coastal areas (Stojanovic & Farmer 2013). Indeed, more than 66% of the worldwide population lives closer than 100 km to a coast (Nicholls et al. 2007). However, many coastlines and beaches are eroding due to different factors such as increased storminess, tectonic subsidence, eustatic sea-level rise and decreased shoreward sediment movement from the shelf associated with leakage out of the beach compartments and human interference (Bird 1981).

Sandy shorelines are very dynamic zones at different time scales (Stive et al. 2002) and their morphology can vary on a short time scale (days, weeks). For instance, Cohn et al. (2017) show that over a six week period, intertidal sandbars can migrate onshore resulting in an increase of the beach width of up to 20 m on the U.S. Pacific Northwest coast. Driven by combined wave and

tidal processes, intertidal bars can migrate landward at rates of 10 m/day (Masselink et al. 2006). Furthermore, Masselink & Pattiaratchi (2001) indicate that morphological changes in Western Australia can happen on a seasonal scale. These morphological changes appear via sediment exchange, that can occur transverse to the beach. For instance, on embayed beaches, the presence of large headlands traps alongshore--moving sediment, resulting in net erosion/accretion at the updrift/downdrift ends of the beach. Since this updrift/downdrift sediment exchange effectively results in clockwise or counterclockwise movements of the shoreline, this process is commonly referred in the literature as beach rotation and is observed on many coastlines.

Shoreline rotation on beaches is based on alongshore sediment exchanges and can represent up to 26% of the shoreward variability of the beach (Harley et al. 2011b). This natural phenomenon does not require a loss or gain of sediment by the system. It is defined as the shoreline movements per unit alongshore distance (Bryan et al. 2013). This alongshore sand transport between opposite extremities of headland embayed beaches is attributed to periodic or long-term changes in wave climate, especially in wave direction (Short & Masselink 1999). Beach rotation appears as a key process for understanding the morphodynamics of embayed beaches. It occurs as a fast response to storms and during the recovery to a more stable orientation after storm events (Ojeda & Guillén 2008). For instance, Short et al. (2001) studied the beach systems in the Sydney region and evidence that beach rotation occurs when southerly waves dominate during the storm season.

Previous studies have already analyzed the behaviour of embayed beaches on a timescale shorter than a year. For instance, Robinet et al. (2020) highlight that cross-shore transport occurs on hourly to monthly timescale while beach rotation operates more gradually on annual and interannual scales. Furthermore, previous studies demonstrated that beach rotation along the NSW coastline occurs on a yearly time-period (Short & Masselink 1999, Short & Trembanis 2004, Harley et al. 2011b) while beach rotation on a short-time scale has only been studied outside Australia (da Fontoura Klein

et al. 2002, Thomas et al. 2011b). To fill this gap, we provide the first analysis focusing on morphologic adjustments of Stanwell Park Beach, NSW, Australia during summer and autumn in the southern hemisphere during an El Niño-Southern Oscillation (ENSO) event. This particular beach has only been studied in detail over the long term. Between 1890 and 1980, Bryant (1983a) showed a minor net erosion of less than 5 m at Stanwell Park Beach with different periods of erosion and accretion. Moreover, regional sea-level variation along this beach can be linked with a hemispheric climatic variation such as the Southern Oscillation (Bryant 1983b) but also with sunspot and moon cycles (Bryant 1984b). Usually beach erosion is associated with storms and sea-level rise, but rainfall is also involved in erosion and has been shown to be an important factor at Stanwell Park Beach on the long-term (Bryant 1985). Furthermore, Bryant (1988) indicates that an increase of 1 m in storm wave height might shift the high tide line by 0.47 m shoreward at Stanwell Park Beach.

The primary aim of this study is to examine short-term changes (days, weeks) to the morphology of the subaerial beach of Stanwell Park Beach and any factors that may influence its behaviours. The study was conducted between February and May 2016 using regular surveys using Real-Time Kinematic Global Positioning System (RTK-GPS) to visualize beach topography.

## METHODS

### LOCATION OF THE STUDY

The NSW coast is characterised by many embayed sandy beaches with alternating rock headlands. Stanwell Park Beach is located 30 km south of Sydney (Figure S1). It is a South-East oriented beach with an alongshore orientation of 42°N and a self-contained sediment budget (Bryant 1985). The beach is dominated by a rhythmic offshore bar and channel system which dissipates wave energy across a wide surf zone. This site can then be considerate as a high energy intermediate beach according to the beach state classification of Wright & Short (1984). Its typical state is either "Longshore Bar Trough" (LBT), "Rhythmic Bar and Beach" (RBB) or "Transverse Bar and Rip"

(TBR). The first two states can develop from an antecedent dissipative profile in an accretionary sequence (Wright & Short 1984). The third state most commonly develops in accretionary sequences when the horns of pre-existing crescentic bars weld to the beach (Wright & Short 1984). The configuration of Stanwell Park Beach can quickly change, with offshore bars migrating shoreward and welding to the beachface within days to months. From our dataset we estimate the beach closure depth being 13.6 m.

The NSW coast experiences a swell regime characterized by a highly variable wind-wave climate superimposed on persistent long-period South-East swell 60% of the time. The wave climate can be defined as high energy with an average wave period of 7.98 s and average wave height of 1.59 m (Short & Trenaman 1992). During winter, storms can occur with significant wave heights of up to 5.5 m and 9.2 m with return periods of approximately 1 year and 50 years, respectively. The tide on this coast is semi-diurnal, with a mean spring range of 1.6 m typical of a microtidal environment (Wright & Short 1984). The beach length is approximately 900 m long, and is characterised by a human-modified sand dune in the central alongshore position. Moreover there are two lagoons fed by freshwater creeks, one at the northern end and On Stanwell Park Beach, rainfall accounts for 12.4% of the variance of the long-term high-tide position (Bryant 1985). The sand is medium sized and sediment had less than 5% shell carbonate and consisted of iron-stained quartz with 10% sub-angular metamorphic fragments (Bryant 1984a).

## BEACH SURVEYING

The topography data were collected using a RTK-GPS in a three-dimensional system. GPS is a satellite-based positioning system developed by the U.S. Department of Defence to provide continuous, worldwide, all-weather navigation (Morton et al. 1993) but the accuracy of a standard GPS is not good enough for beach surveys. RTK-GPS, however, uses more sophisticated error correcting techniques that makes it suitable for surveying beach dynamics (Harley et al. 2011a). In RTK-GPS, a computer box calculates its position relative to a fixed, known GPS receiver. Both receivers

measure their position using the higher frequency satellite signals (Harley et al. 2005). As the base station's coordinates are known, it can then calculate the degree of errors in the GPS measurements. These error corrections are transmitted in real-time to the computer box, which can then calculate its absolute position with accuracy in the order of a few centimetres. This survey method is well known for studying beach topography and is used in many studies (Haxel & Holman 2004, Pardo-Pascual et al. 2005, Thomas et al. 2010, Miller et al. 2011). To measure beach topography on a local scale, a series of 6 cross-shore survey transects were established at Stanwell Park Beach with an averaged distance of 170 m between each profiles (Figure 1). Furthermore, the beach is divided in 3 zones to study precisely the estimation of sand volume over time.

Surveys at Stanwell Park Beach were made by walking with the RTK-GPS mounted on a backpack. The walking surveys were accomplished with the person walking perpendicular down the beach, until waist-depth, to obtain cross-shore transects and then walking diagonal up the beach. Each survey took approximately 1.5 hours to complete and were conducted around low tide to cover as much distance offshore as possible. However, the surveys only cover the subaerial section of the beach, the sub-marine part was not surveyed.

Over 4 months, 10 surveys were conducted, the first one on 10th February, 2016 and the last one on 14th May, 2016 (Table 1).

## THREE-DIMENSIONAL BEACH SURVEYS

The first step before creating topographic maps is to interpolate the data. During this study the interpolated grid has a 1 m mesh. The interpolation function used is based on a Delaunay cubic triangulation (Lee & Schachter 1980) that produced a smooth surface, enabling the attainment of regular data. Consequently topographic maps are generated with the x-axis being the cross-shore axis and the y-axis being the alongshore axis. The zero axes origin are a default offset of the software used to analyse the data. The origin of the y-axis represents the southern end and the maximum of the y-axis represents the northern head of the beach. The zero elevation on the topographic maps
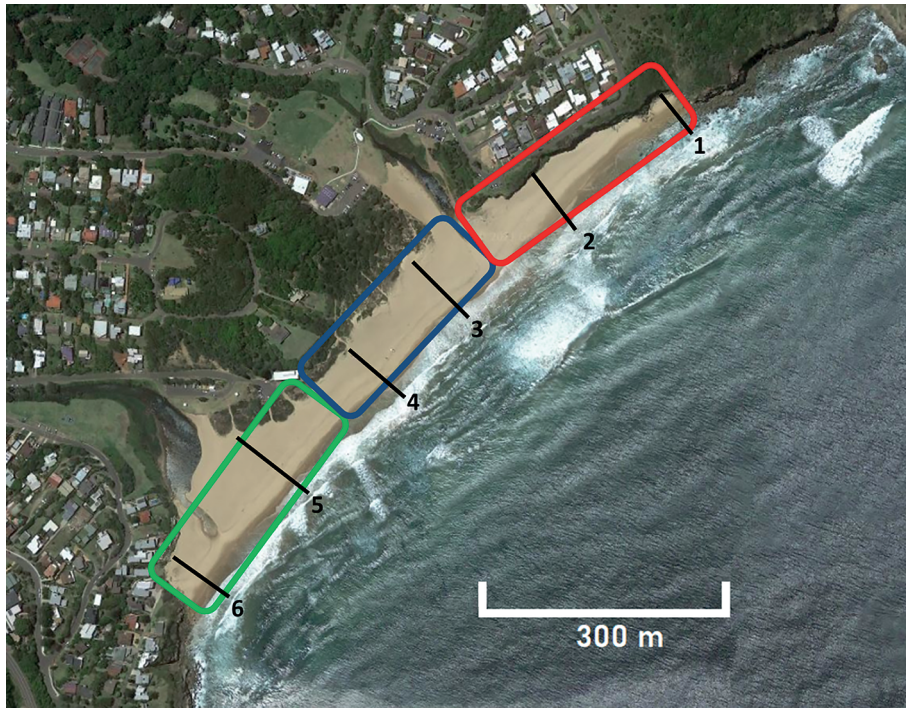
**Figure 1.** Location of the cross-shore profiles. Green box is the southern end of the beach, blue box is the middle of the beach and red box is the northern part (source Google Earth on 03/12/2018).

**Table 1.** Date of the surveys and tide range.

| Date | Tide range (m) |
| --- | --- |
| 10th February (survey 1) | 0.15 |
| 05th March (survey 2) | 0.49 |
| 10th March (survey 3) | 0.16 |
| 20th March (survey 4) | 0.44 |
| 24th March (survey 5) | 0.43 |
| 07th April (survey 6) | 0.21 |
| 15th April (survey 7) | 0.55 |
| 22nd April (survey 8) | 0.5 |
| 05th May (survey 9) | 0.29 |
| 14th May (survey 10) | 0.57 |

refers to the zero defined by the World Geodetic System 1984 (WGS84). To evaluate elevation change between two successive beach surveys, the elevation of the first survey is subtracted from the second survey. This method provides a visual map of the morphologic differences (erosion and accretion) between the two surveys.

Sand volume is calculated over the subaerial beach to provide an indicator of net erosion and accretion through time (Theuerkauf & Rodriguez 2012) and can be calculated by:

$$B_i = A_0 \Sigma (Z_i - Z_0) \qquad (1)$$

Where $B_i$ is the sand volume for a given survey, $A_o$ is the area of the beach for the reference day in square meters, which is the 10th February, 2016 (Table 1), $Z_i$ is the elevation for the given survey day in meters and $Z_o$ is the elevation for the reference day in meters. The sand volume was calculated for the entire subaerial beach but also for three equal parts of the beach: northern part, the middle of the beach and the southern part (Figure 1). To estimate sand transport between sequential surveys, we use the method of Dail et al. (2000).

## CROSS-SHORE PROFILES

In order to examine the behaviour of the beach in more detail at certain locations, cross-shore profiles were extracted from the interpolated topography. During this study 6 cross-shore profiles were made for each survey day with Profile 1 at the northern part of the beach and Profile 6 at the southern part (Figure 1). The location of these profiles was chosen to capture the northern and southern ends of the beach and locations in between. The alongshore distances were not equal due to

the presence of the two lagoons. The zero x-axis origin is a default offset of the software used for the analysis and the y-axis represents the elevation.

## Offshore wave data

Wave data used for wave forcing analyses were obtained from the Port Kembla directional waverider buoy located in 80 m water depth, 12 km offshore of Port Kembla and 26.5 km south of Stanwell Park Beach (Figure S2). Data is provided from the Manly Hydraulics Laboratory (MHL) and are collected under the NSW Coastal Data Network Program managed by the Office of Environment and Heritage (OEH). The buoy takes hourly measurements of the significant wave height ($H_s$), zero crossing period ($T_z$), wave direction ($\theta$) maximum wave height ($H_{max}$) as well as peak wave period ($T_p$). In a previous study (McCarroll et al. 2016), a good correlation in wave heights was found between Sydney wave buoy and Port

Kembla wave buoy suggesting both are representative of wave conditions offshore of the beaches between these two buoys. Failure of the Port Kembla buoy occurred during the study period which is why wave data is incomplete (Figure 2). It fails 2 days during P3 (Table 2) and 5 days during P5.

In order to analyze the swell condition during the study period, we look for storm events in our wave dataset. A storm event is an event where $H_s$ exceeds the 0.95 quantile (Masselink et al. 2014), which represents 2.85 m for Port Kembla data. The initiation of a storm was defined as the time when the hourly-averaged $H_s$ exceeded the 0.75 quantile (Masselink et al. 2014), being 1.72 m for Port Kembla data, and the end of the storm was the time when the hourly-averaged $H_s$ return below 1.72 m. With these offshore wave parameters, we can calculate the incident energy flux ($F_b$) which is an expression of the incident energy level of the waves
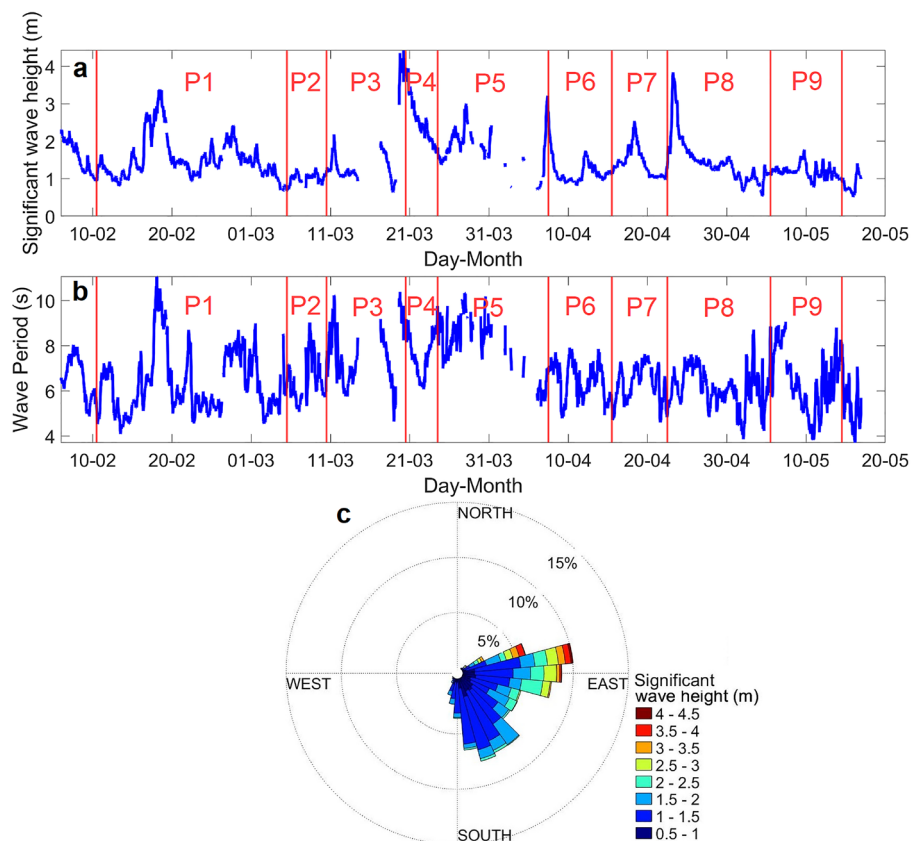


**Figure 2.** Swell conditions for the entire study period: (a) Significant wave height; (b) Mean wave period; and (c) Wave direction. Gaps in the data are due to temporary drop-outs of the waverider buoy.

**Table 2.** The nine study periods between 10th February and 14th May.

| Period 1 (P1) | 10th February - 05th March |
|---|---|
| Period 2 (P2) | 05th March - 10th March |
| Period 3 (P3) | 10th March - 20th March |
| Period 4 (P4) | 20th March - 24th March |
| Period 5 (P5) | 24th March - 07th April |
| Period 6 (P6) | 07th April - 15th April |
| Period 7 (P7) | 15th April - 22nd April |
| Period 8 (P8) | 22nd April - 05th May |
| Period 9 (P9) | 05th May - 14th May |

(Dail et al. 2000). The greater the value of $F_b$, the stronger will be the impact of the waves on the beach. This indicator can be calculated by:

$$F_b = \frac{\rho g^2}{16\pi} H_s^2 T_{mean} \qquad (2)$$

Where $F_b$ is the incident energy flux, $\rho$ = 1025 kg/m³ is water density, g = 9.81 m/s² is gravitational acceleration, $H_s$ is the significant wave height in meters, $T_{mean}$ is the average period in seconds.

## Beach rotation

Beach rotation is directly linked to the alongshore component of wave energy flux ($P_y$) which is linked to the significant wave height (Biausque et al. 2016). Positives values indicate that the southern end of the beach is moving offshore and negative values indicate that the northern end of the beach is moving offshore. Values close to zero denote an un-rotated state of the beach. The alongshore component of wave energy flux, used as a proxy of beach rotation, can be calculated by:

$$P_y = \frac{\rho g^2}{32\pi} H_s^2 T_{mean} \, sin\left(\theta_{mean}\right) cos\left(\theta_{mean}\right) \qquad (3)$$

where $P_y$ is alongshore component of wave energy flux, $\rho$ = 1025 kg/m³ is water density, g = 9.81 m/s² is gravitational acceleration, $H_s$ is the significant wave height in meters, $T_{mean}$ is the average period in seconds and $\theta_{mean}$ is the angle of wave approach relative to the beach orientation in radians. To compute the last parameter, it is necessary to subtract shore-normal direction of the waves (132°) to the wave direction. We use deep water waves to

calculate the wave energy flux because we consider that the bathymetry varies slowly and thus the onshore component of the wave energy flux is conserved (Longuet-Higgins 1970). Furthermore we consider that the bathymetric contours are linear and parallel from deep water to the shore. With these two assumptions and via Snell's law, $P_y$ is conserved outside the surfzone.

Moreover, the alongshore component of radiation stress ($S_{xy}$) can also be used for beach rotation (Ojeda & Guillén 2008). As beach rotation is caused by alongshore sediment transport, it is expected that large (positive or negative) values of this parameter will be related to episodes of beach rotation while low values will imply predominance of cross-shore sediment transport and therefore no changes in the beach orientation.

This parameter is calculated following Komar (1976):

$$S_{xy} = \frac{1}{16} \rho g H_s^2 \, sin\left(\theta_{mean}\right) cos\left(\theta_{mean}\right) \qquad (4)$$

Where $S_{xy}$ is the alongshore component of radiation stress, $\rho$ = 1025 kg/m³ is water density, g = 9.81 m/s² is gravitational acceleration, $H_s$ is the significant wave height in meters and $\theta_{mean}$ is the wave angle with respect to the shore-normal direction in degrees. As previously stated, deep water waves parameters are used because we consider that the bathymetry varies slowly, thus the bottom friction change is negligible.

As a consequence, the radiation stress remains constant from deep water to the breaking point (Stive & Wind 1982).

## Rainfall data

We obtained rainfall data from the Australian Government Bureau of Meteorology (BOM). The station used for this study is Darkes Forest rainfall station, located 6.3 km to the west of Stanwell Park Beach (Figure S2).

The elevation of the station is 370 m. Rainfall is linked to discharge of the creeks which can contribute to the opening of the two lagoons on the beach and therefore can play a role in the morphology of the study site. Opening of the lagoons during heavy rains can introduce sediment to the surf zone.

# RESULTS

## HYDRODYNAMIC

During the whole study period, significant wave height did not exceed 4.5 m (Figure 2a) and the maximum wave period was about 11 s (Figure 2b). Wave direction was dominated by South-East swell with a mean wave direction of 121°, a maximum wave direction of 203° and a minimum wave direction of 48° (Figure 2c). Significant wave heights of waves coming from East were ~2.5 m larger than waves coming from the South. Using the storm criteria of Masselink et al. (2014), 41 'storm' events were identified over February 2016 and mid-May 2016 and the mean storm duration was 13 hours. The mean 'storm' wave height was 3.37 m and the mean 'storm' wave period was 8.1 s. However, many of these events were associated with non-storm weather conditions and were primarily swell events, there were no real 'storm' events associated with major climatic cyclonic disturbances. Therefore, despite using the criteria of Masselink et al. (2014), there was no significant storm wave activity during the study period, it was generally a calm period. In order to better understand the morphologic changes between surveys, the wave data has been split into nine discrete temporal periods between each survey as shown in Table 2 and indicated on Figure 2.

Maximum wave height over the study period was during P3 with maximum waves of 4.4 m, but the highest mean significant wave height was during P4 with 2.6 m (Table 3). Maximum mean wave period was associated with P5, with a period of 8.1 s but maximum wave period was during P1 with a value of 11.1 s.

Mean swell direction was maximum during P4 with a direction of 148° (South-East). In general, waves were more from the South during this period than any other time in the study. Maximum wave direction was during P1 with 203°. Of note, P1 and P2 are important for this study as waves were higher and wave direction is more important during P1 (respectively 3.4 m and 203° for the maximum) than during P2, but mean wave periods were similar for these two periods.

## BEACH CHANGE OVER THE WHOLE STUDY PERIOD

During the study period, the whole subaerial beach did not behave in a similar way. Zones of minor accretion are situated on the upper beach near the northern headland and towards the middle of the beach (Figure 3 and 4). These zones display crescentic shaped embayments similar to those caused by rip currents (Castelle et al. 2015). Moreover, the erosion process dominates on the southern end of the beach during the whole study period, with a maximum elevation loss of 2 m. The rest of the beach does not have significant changes, with topographic changes lower than 50 cm. The cross-shore profiles provide more detail on the morphologic evolution at each location between the original and final state of the subaerial beach (Figure 4). In addition, these profiles allow quantification of the elevation difference between different cross-shores profiles. Profile 1 at the northern part of the beach, shows an elevation loss during the study period. At the lower, seaward end of the profile this loss is ~1 m (Figure 4a). On Profile 2, the cross-shore profiles look similar between each others with small changes over time (Figure 4b). In the middle of the beach on Profiles 3 and 4, the upper beach elevation increases by

**Table 3.** Parameters for each period of the study: Hs = significant wave height; T = period of the swell; and D = direction of the swell.

|  | P1 | P2 | P3 | P4 | P5 | P6 | P7 | P8 | P9 |
|---|---|---|---|---|---|---|---|---|---|
| **Hs max(m)** | 3.4 | 1.3 | 4.4 | 4 | 3.2 | 2.7 | 2.5 | 3.8 | 1.8 |
| **Hs mean (m)** | 1.5 | 1 | 1.6 | 2.6 | 1.8 | 1.2 | 1.4 | 1.5 | 1.2 |
| **T max (s)** | 11.1 | 9.2 | 10.4 | 9.2 | 10.3 | 7.9 | 7.6 | 8.7 | 9.1 |
| **T mean (s)** | 6.4 | 6.5 | 7.5 | 7.6 | 8.1 | 6.4 | 6.3 | 6.1 | 6.5 |
| **D max (°)** | 203 | 162 | 185 | 179 | 200 | 175 | 189 | 194 | 183 |
| **D mean (°)** | 116 | 109 | 122 | 148 | 142 | 124 | 106 | 103 | 117 |
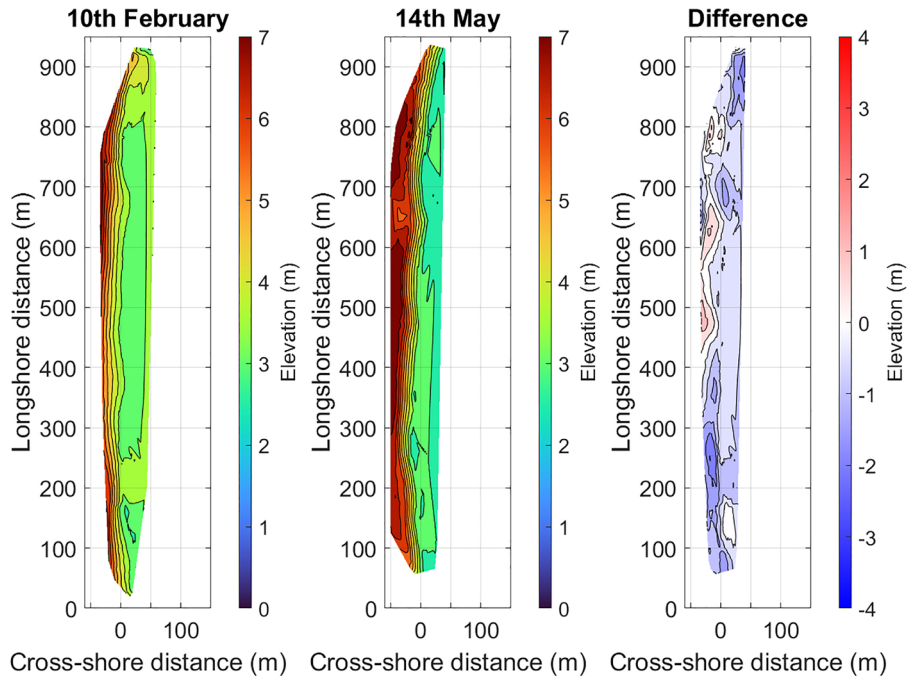
**Figure 3.** Topographic change on Stanwell Park Beach between 10th February and 14th May.
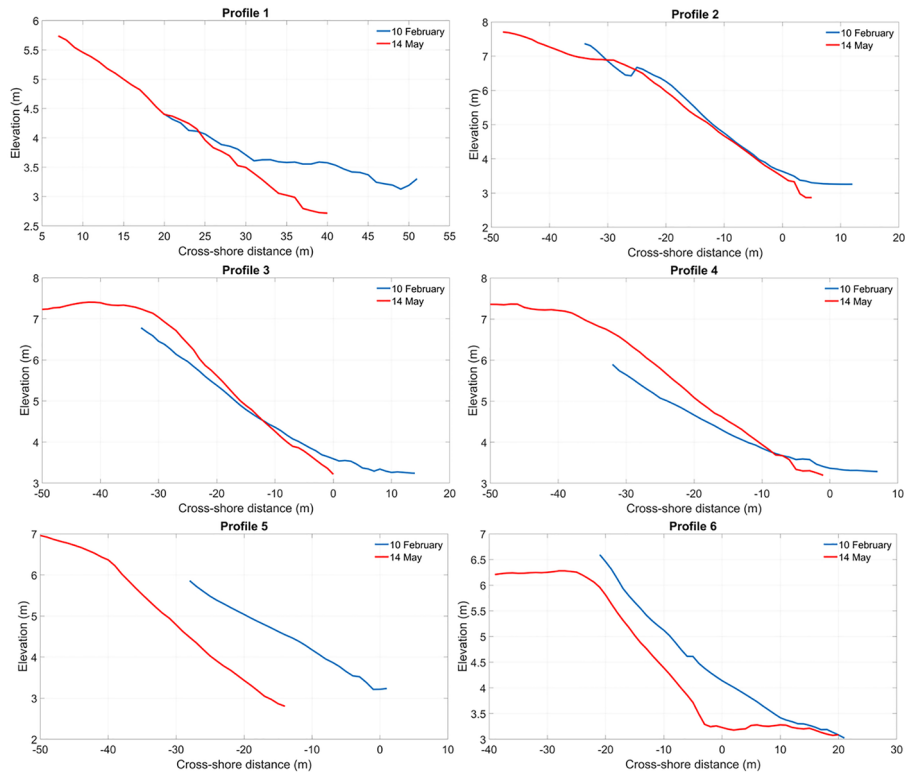


**Figure 4.** The six cross-shore profiles on 10th February (blue line) and 14th May (red line): (a) Profile 1; (b) Profile 2; (c) Profile 3; (d) Profile 4; (e) Profile 5; and (f) Profile 6.

~1 m at the end of the study period compared to the beginning of the study period, meaning that the upper beach gained sediment over time (Figure 4c and 4d). On Profiles5 and 6, at the southern end of the beach, the 10th February cross-shores profiles are higher than the 14th May profiles, indicating a loss of sand (Figure 4e and 4f). The lower part of the beach was more impacted with an elevation loss of more than 1 m. In summary cross-shore profiles (Figure 4) show a loss of sand at the northern and southern ends of the subaerial beach while the middle of the subaerial beach gained sediment during the study period, especially on the upper beach. Topographic maps (Figure 3) show an unaffected change on the southern end of the subaerial beach while cross-shore profiles 5 and 6 (Figure 4e and 4f) show local erosion on the lower beach. This could be explained by the fact that profiles show change to particular areas while maps provide an overview of the whole subaerial beach.

However, these findings cannot be applied to all the study periods and the following section provide more details on the morphologic changes over the different study periods.

### BEACH MORPHODYNAMICS

Stanwell Park Beach experiences significant and rapid erosion and accretion of the beachface. Like other steep beaches (Wright et al. 1979), the most common profile configuration includes a well-developed berm, a steep beachface and weak longshore variability. Due to length constraints, only maps of particular interest are shown here (Figures 5, 6 and 7). For a specific period, the sedimentary processes are not spatially-uniform along the entire subaerial beach. Moreover, these processes are not uniform in time meaning that a specific beach area can have a low elevation (loss of sand) followed by a higher elevation (gain of sand) just a few days later. Sedimentary processes therefore
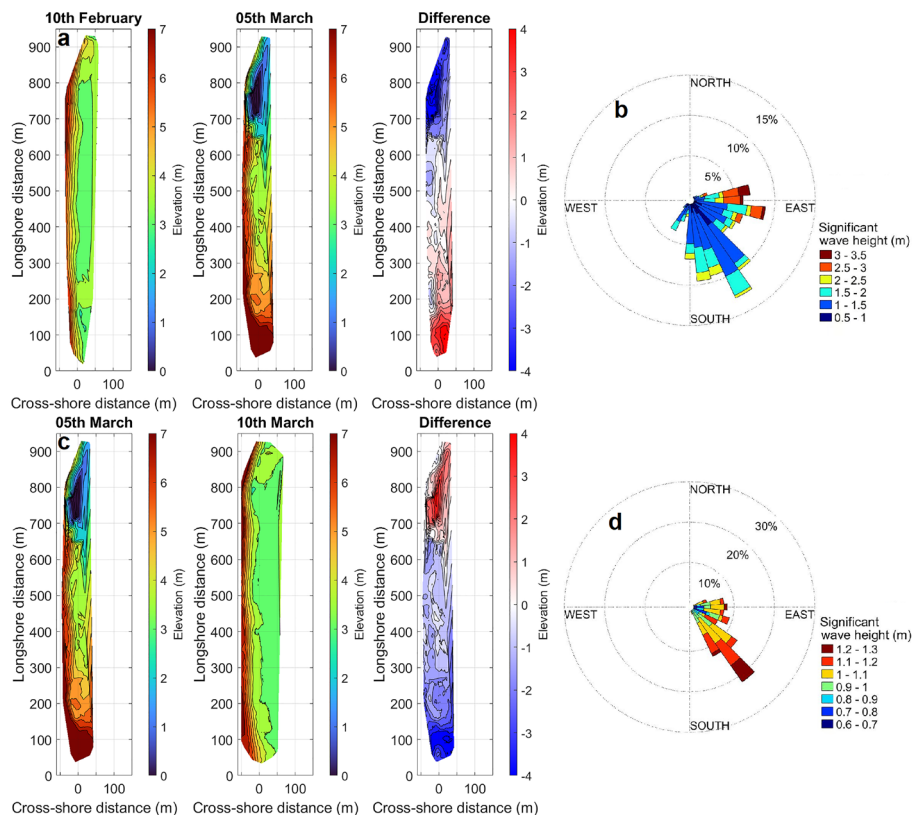


**Figure 5.** Visualization of beach rotation event between 10th February and 10th March. (a) Topographic maps of Period 1. (b) Wave conditions of Period 1. (c) Topographic maps of Period 2. (d) Wave conditions of Period 2. Note that the percentage on panel (b) and (d) are different.
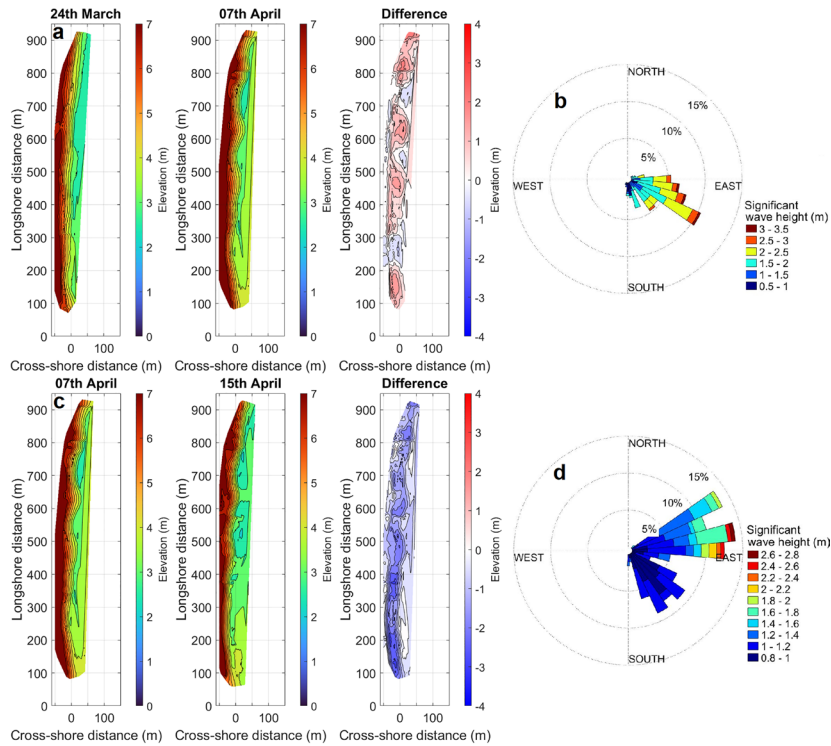
**Figure 6.** Visualization of embayment of rip channels: (a) Topographic maps of Period 5. (b) Wave conditions of Period 5. (c) Topographic maps of Period 6. (d) Wave conditions of Period 6.
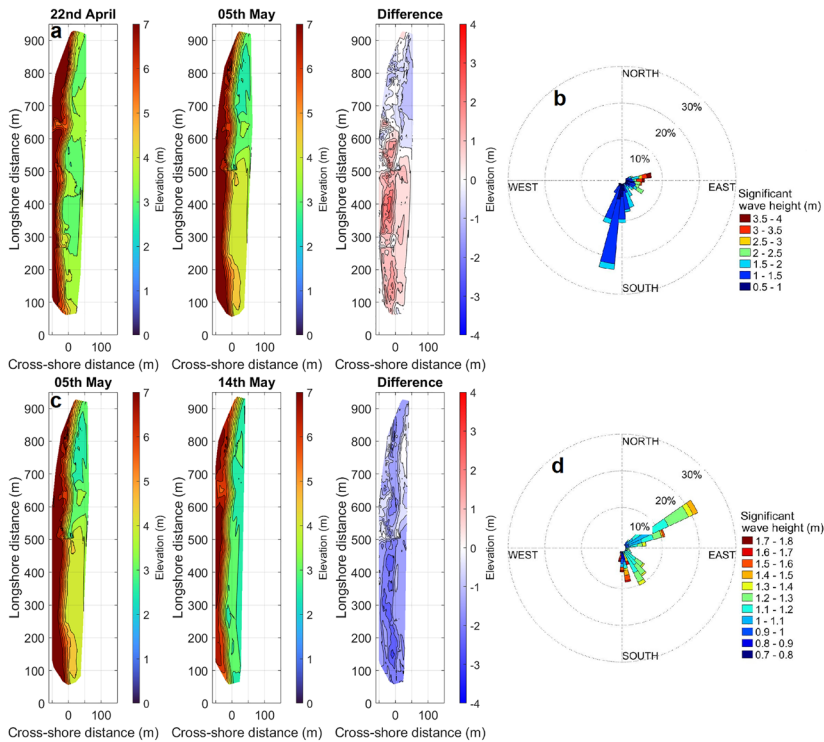


**Figure 7.** Topographic maps resuming Stanwell Park Beach behave during study period: (a) Period 8 with (b) respective wave direction; and (c) Period 9 with (d) respective wave direction.

vary in time and space. Looking at all the different maps (Figures 5, 6 and 7); we observe the morphologic behaviour along the entire subaerial beach over short time scales. Regardless of whether it was the lower or upper beachface, sedimentary movements along Stanwell Park Beach occur continuously.

The study period between survey 1 and survey 3 is particularly interesting as it shows a beach rotation (de Alegria-Arzaburu & Masselink 2010, Thomas et al. 2011a, Turki et al. 2013, Thomas et al. 2015). Wave dynamics during P1 is characterized by waves higher than 3 m coming from the East (Figure 5b). This particular hydrodynamics conditions are associated with large erosion (-4 m) at the northern part of the subaerial beach and at the same time large accretion (4 m) at the southerly part. Sand seems to have moved from the northern part to the southern part of the subaerial beach during this period. In contrast, the period P2 evidences calm conditions with maximum waves of 1.2 m coming from the South (Figure 5d). These hydrodynamics conditions are associated with a gain of sediment (about 3 m) in the northern part of the subaerial beach while the southern part of the beach experiences a loss of sediment (about -3 m). During this period, sand seems to move towards the North.

During P5 several elevated areas with a crescent shape are evident on the 07th April map (Figure 6a).

These same morphologic features are also evident on the topographic difference map where elevation is high, indicating accretion of ~1.5 m during P5. These particular forms on the beachface are the embayments of rip channels (Castelle et al. 2015). During this period, large waves (mean Hs = 1.8 m) come from the East/South-East, with a perpendicular direction to the beach. During P6, the crescentic forms have disappeared and important erosion zones appear (Figure 6c). During this period the wave direction is similar to the previous period but the wave height is smaller (mean Hs = 1.2 m). This result evidences that the crescentic forms appeared in only two weeks and disappeared rapidly.

Topographic maps of P8 and P9 can resume the behaviour of Stanwell Park Beach during the study period (Figure 7). During P8, large accretion areas located from the southern end to the middle of the subaerial beach of ~1 m appear. In contrast, the northern end loose sediment during this period (about -1 m). Southerly waves are dominant during P8 but they are rather small whereas waves coming from the East are large (maximum Hs of 4m). Similarly to P1 (Figure 5a), P8 highlights a beach rotation due to the large waves coming from the East. During P9, the entire subaerial beach loose sediment (Figure 7c). The previous accretion area on the southern end of the subaerial beach seen on Period 8 has disappeared. Additionally, during P9 small waves from the East are dominant with maximum Hs of 1.5 m.

## BEACH ROTATION AND SEDIMENT VOLUME

The values of the alongshore component of wave energy flux (Figure 8a) are high and positives during P1, P4, P7 and P8, with a maximum of 85 kW/m during P4. These values indicate that the southern end of the beach moves offshore. However the field observations and topographic maps show only a beach rotation between P1, P2 and P8. As a consequence, this index, for the present study, is not completely related with the data and field observations. One reason could be that the database is too short (only 4 months) to encompass significant results. Others studies showing good results for this beach rotation proxy use databases spanning years and do not use RTK-GPS to study beach dynamics (Komar & Inman 1970, Van de Lageweg et al. 2013, Biausque et al. 2016).

Large (positive or negative) values of mean alongshore component of radiation stress are related to episodes of beach rotation. For all periods the value of this parameter is close to zero except for P2 and P8 which had a value of -86 N/m and -48 N/m, respectively (Figure 8b). These values indicate that during P2 and P8, a beach rotation event occurs while during all the others periods cross-shore sand transport is dominant. This is rather consistent with topographic maps observations during P2 and P8. For our study, the mean alongshore component of radiation stress is in better agreement with our topographic observations and hydrodynamic database than the alongshore
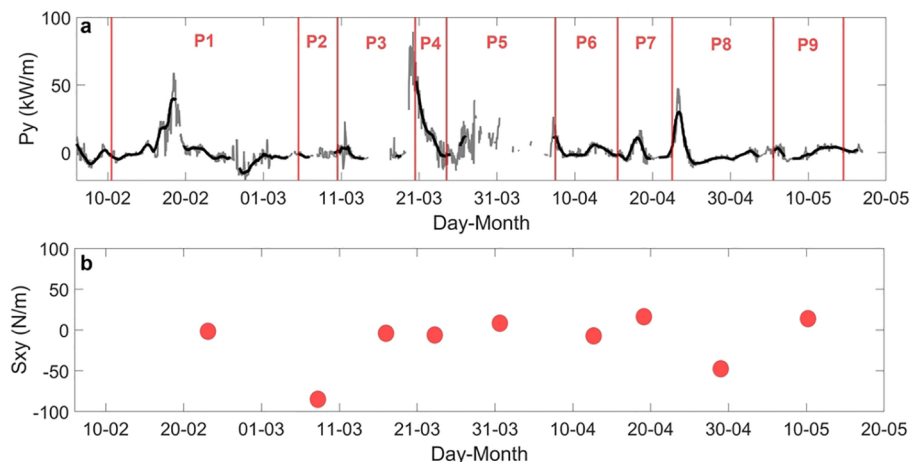
**Figure 8.** Time series of beach rotation index: (a) Alongshore component of wave energy flux. Red lines indicate survey day and black line indicates one day average; and (b) Mean alongshore component of radiation stress for each period.

component of wave energy flux, that do not behave as expected.

The different observations described previously must be related with subaerial beach volume calculated from RTK-GPS surveys. The zero reference day, when sand volume along all profile lines is zero, is the first day surveyed — 10th February. The different subaerial beach areas represented on Figure 9a are defined on Figure 1. Sand volume variations for the entire subaerial beach and the middle part of the beach are essentially similar with a difference of magnitudes. Sand volume diagram indicates that the subaerial beach has globally lost sand during the study period, a loss about $2 \times 10^4$ $m^3$ (Figure 9a). During P1 it is possible to observe a northerly loss of sediment of $2 \times 10^4$ $m^3$ and a southerly gain of about $1.9 \times 10^4$ $m^3$ (Figure 9a).

During P2 the reverse phenomenon happens, with a southerly loss of sediment of about $1.7 \times 104$ $m^3$ and a northerly gain of about $2.1 \times 104$ $m^3$ (Figure 9a). These observations are in agreement with the observed beach rotation between survey 1 and 3. At the end of the study, for these two parts of the subaerial beach, sand volume is almost similar as at the beginning of the study but these two parts of the subaerial beach have not behaved the same way during the study period.

The estimation of sand volume flux provides an indication of the rate of erosion and accretion (Dail et al. 2000). It estimates what time period has the highest gain or loss of sediment per day for

the entire subaerial beach (Figure 9b). It should be noted that these are averages and it would be expected that much higher or lower instantaneous rates occur between surveys. The highest gain of sand occurred during P3, just after the beach rotation event, with a gain about $5 \times 10^3$ $m^3$/day relative to reference day (10th February).

The highest loss of sediment occurred during P9 with a loss about $7 \times 103$ m3 /day and this high loss of sand can be correlated with high incident energy flux (Dail et al. 2000). Indeed, if the incident energy flux is high, waves will have a large impact on the subaerial beach and erosion will happen. The highest loss of sediment, occuring during P9, happens when the incident energy flux is high, with a value of 3.2x105 kg/s (Figure 9c).

Looking at the whole study period, high losses of sand occur just after a high incident energy flux, illustrating the effect of the waves on the subaerial beach.

## EFFECT OF RAINFALL ON THE BEACHFACE

During the study period, the rainiest month was March (total = 79.2 mm; Table 4) which also had the highest day of rain (21.6 mm on 16th March). The driest month was May (total = 14.0 mm). However, according to data from the Australian Bureau of Meteorology, the year 2016 was a dry year with low rainfall. This phenomenon is presumably caused by ENSO cycle during the year 2016 (You & Lord 2008). As such, the lagoons have remained
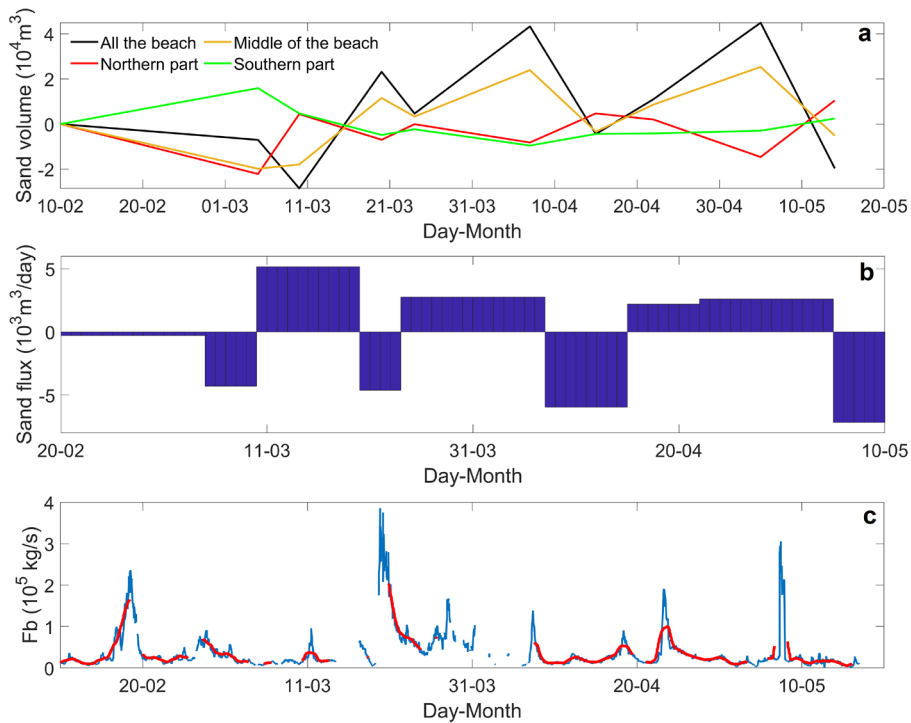
**Figure 9.** Sediment volume proxies: (a) Sand volume variations. Black line is sand volume for the entire beach, red line is the sand volume for the northern part, blue line is the sand volume for the middle of the beach, green line is the sand volume for the southern end; (b) Average sand flux per day between surveys for the entire beach; and (c) Incident energy flux. Red line indicates 36 hours average.

**Table 4.** Rainfall data for each month of the study period.

|  | February | March | April | May |
|---|---|---|---|---|
| **Highest daily (mm)** | 13.2 | 21.6 | 21.0 | 9.6 |
| **Monthly total (mm)** | 47.4 | 79.2 | 52.2 | 14.0 |

mostly closed to the ocean by a well-developed berm. In terms of daily rainfall observations (Figure 10c) it is important to note that April 19th was a day of heavy rain just three days before a beach survey conducted on April 22nd. During this day rainfall was 21.6 mm, making it the rainiest day of April 2016 and the second rainiest day of the study period. By examining the topographic map for April 22nd (Figure 10a), it is evident that the rain event had an impact on the morphology of the subaerial beach. On this map, a low elevation is visualized on the upper beach due to the opening of the lagoon, at y = 650 m where the north lagoon is located (Figure 10b).

## DISCUSSION

This study examines topographic and hydrodynamic data for Stanwell Park Beach between February and May 2016. Our data only cover the subaerial section of the beach therefore we could not study the sub-tidal extents of the beach. As a consequence, the total sediment budget approach could not be analyzed and thus the total geomorphic response could not be fully described. In terms of hydrodynamics it is possible to note that the study period was calm without large storm events. These calm wave conditions are related to ENSO, which decrease the incidence of tropical cyclone activity off eastern Australia during what

is normally the maximum activity period (February-March), causing the observed relative decrease in wave power impacting the Sydney region during this study (Phinn & Hastings 1992). However despite these calm conditions Stanwell Park Beach was still a very dynamic environment during the study period, with sand moving on a short-time period. This result means that the behaviour measured does not necessarily need storm events to blossom.

Analyses of topographic maps, mean alongshore component of radiation stress and beach sand volume indicate two dominant type of morphologic response during this time period. First, eastern waves tend to drive longshore transport causing a complete beach rotation during P1 (anticlockwise rotation) followed by a beach restoration, reaching an equilibrium during P2 (clockwise rotation). The phenomenon of beach rotation is not unusual for an embayed beach, but has only been shown to occur on a short-time scale outside Australia (da Fontoura Klein et al. 2002, Thomas et al. 2011b). For the first time, we demonstrate that short-time beach rotation occurs along the NSW coastline. The most important parameter controlling beach rotation is wave direction, with large waves coming from the East (Figure 5b). However, Short et al. 2001) indicate that beach rotation predominately occurs with southerly waves on beaches of the Sydney region. This difference in wave direction, leading to beach rotation, between our study and Short et al. (2001) is due to the different orientation of the beach. The second morphologic response is waves with a perpendicular direction to the beach tending to create rip current embayments and rip current channels, promoting offshore sediment transport (Calvete et al. 2005). This is particularly evident during P5 (Figure 6). Rip current channels and rip current embayments are well known morphologies that have already been studied in Australia (Brander 1999, McCarroll et al. 2016) and in other places of the world (Castelle et al. 2015, Borra et al. 2022, Wernette & Houser 2022). Based on the observations of this study, Figure 11 summarizes the behaviour of Stanwell Park Beach under the wave conditions of our study period. This representation does not support the general behaviour of Stanwell Park Beach but only reflects the behaviour of the subaerial beach during the four months of the study period. The representation of the behaviour of the beach shows only erosion phase but Stanwell Park Beach does not suffer from chronical erosion, the accretion phases were not captured by our short-time dataset. To calculate $P_y$ and $S_{xy}$ we use deep-water wave data. However, if we would have used shallow-water wave data, the wave direction would be different due to wave refraction and thus $P_y$ and $S_{xy}$ would also be different.

On 22nd April map (Figure 10), just after a heavy day of rain, a low elevation zone is observed where the north lagoon is located. Rainfall transports sand from the upper beach to the surf zone, creating a sand bar in front of the opened lagoon. Opening lagoon can be a third control on the morphological behaviour of Stanwell Park beach but more research would be necessary to understand exactly how this work.

## CONCLUSIONS

A comprehensive analysis of the dominant processes governing subaerial beach variability at Stanwell Park Beach, NSW, Australia has been undertaken by comparing over four months of weekly subaerial beach survey measurements with both measured and re-analysed offshore wave data. Even without energetic wave conditions, morphologic adjustments in this dynamic environment are rapid with an overall loss of $2 \times 10^4$ m³ of sediment during the study period. However, this general loss of sediment is only true for our study period, the subaerial beach does not suffer from chronic erosion. The recovery phase was not capture during the four months of our study period. Moreover, a beach rotation event has been evidenced during a short-time period of only one month. This event occurs quickly and the subaerial beach can restore itself to an equilibrium state in only five days. During the study period, alongshore sand transport is dominant only 30% of time (P1 and P2) while cross-shore transport is dominant the rest of the time.

Embayed beaches are more complex environment than non-embayed beaches due to the beach rotation phenomenon that can occur. Using weekly RTK-GPS surveys from 10th February until 14th
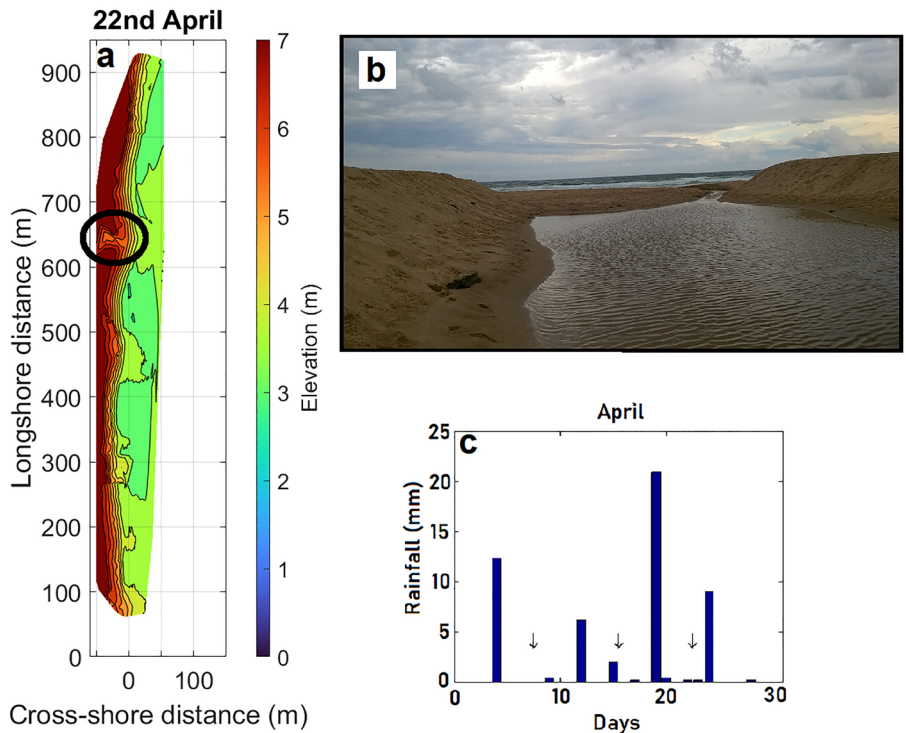
**Figure 10.** Rainfall impact on the beach: (a) Topographic map on 22nd April. Black circle shows the location of the northern lagoon; (b) Northern lagoon opened (photo taken on 22/04/2016); and (c) April daily rainfall. Down arrows indicate the survey days.
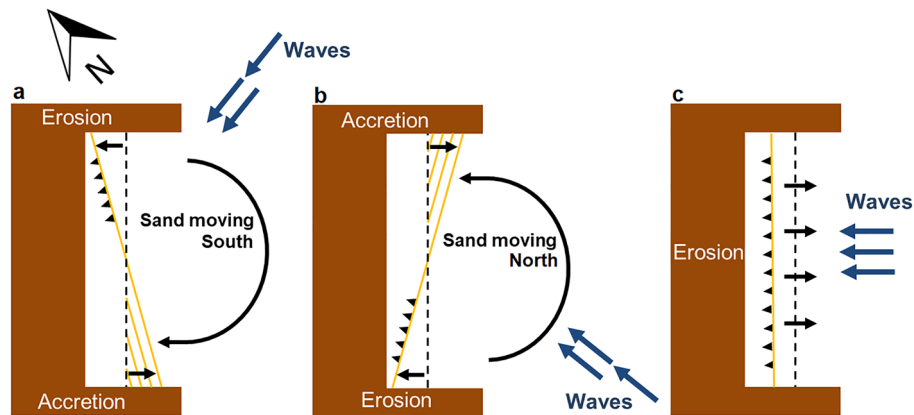


**Figure 11.** Simple model of Stanwell Park Beach behaviour: (a) Waves coming from the East provide beach rotation; (a) Waves coming from the South provide beach rotation; and (c) Waves coming from the South-East provide cross-shore sand transport.

May, we shown that the erosion of an embayed beach is a complicated combination of wave direction, significant wave height, wave period, mean alongshore component of radiation stress, incident energy flux and beach state. Each factor has an effect on other factors and they cannot be studied separately. Moreover, as shown during this study, hydrodynamic forcing is not the only one that plays a role on beach erosion but rainfall can change the beachface, especially for beaches with lagoons that intermittently open and close.

This study has therefore provided a clear demonstration of the sensitivity of embayed beaches to short-term variability in wave climate, even

during low wave energy conditions. Although the offshore storage characteristics of Stanwell Park Beach sediments could not be observed with the RTK-GPS surveys, the beach surveys did extend into the inner surf zone with some evidence suggesting that sediment is distributed offshore in a uniform manner (Dail et al. 2000). An examination of the short (hourly to daily) and long time scale (interannual) beach behavior at this site would be a valuable extension to this study and it could be compared to nearby eastern and Sydney northern beaches study (Ranasinghe et al. 2004, Harley et al. 2011b, McCarroll et al. 2016) and Wollongong beaches (Clarke & Eliot 1988).

## ACKNOWLEDGMENTS

## AUTHOR CONTRIBUTIONS

R.A.: Conceptualization; Investigation; Writing - original draft; Writing - review & editing;

R.W.B.: Conceptualization; Supervision; Project Administration; Writing - review & editing.

## REFERENCES

BIAUSQUE, M., SENECHAL, N., BLOSSIER, B. & BRYAN, K. R. 2016. Seasonal variations in recovery timescales of shorelines on an embayed beach. *Journal of Coastal Research,* 75(spe1), 353–357.

BIRD, E. 1981. World-wide trends in sandy shoreline changes during the past century. *Géographie Physique et Quaternaire,* 35(2), 241–244.

BORRA, S., NAIR, T., JOSPEH, S., KUMAR, S. V., SRIDEVI, T., HARIKUMAR, R., SRINIVAS, K., YATIN, G., GIREESH, B., VENKATESWARARAO, K., ANJANEYULU, A. & PRASAD, K. V. S. R. 2022. Identifying rip channels along RK beach, Visakhapatnam using video and satellite imagery analysis. *Journal of the Indian Society of Remote Sensing,* 1–18.

BRANDER, R. W. 1999. Field observations on the morphodynamic evolution of a low-energy rip current system. *Marine Geology,* 157(3-4), 199–217.

BRYAN, K. R., FOSTER, R. & MACDONALD, I. 2013. Beach rotation at two adjacent headland-enclosed beaches. *Journal of Coastal Research,* 65(10065), 2095–2100.

BRYANT, E. 1983a. Coastal erosion and accretion, Stanwell Park Beach, NSW, 1890–1980. *Australian Geographer,* 15(6), 382–390.

BRYANT, E. 1983b. Regional sea level, southern oscillation and beach change, New South Wales, Australia. *Nature,* 305(5931), 213–216.

BRYANT, E. 1984a. Sediment characteristics of some Eastern Australian foreshores. *Australian Geographer,* 16(1), 5–15.

BRYANT, E. A. 1984b. Sunspot and MN tidal effects on Stanwell Park, NSW, beach change, 1895-1980. *Search*, 15(7-8), 226-228.

BRYANT, E. A. 1985. Rainfall and beach erosion relationships, Stanwell Park, Australia, 1895-1980: worldwide implications for coastal erosion. *Zeitschrift für Geomorphologie N.F. Supplement,* 57, 51-65.

BRYANT, E. A. 1988. Storminess and high tide beach change, Stanwell Park, Australia, 1943–1978. *Marine Geology,* 79(3-4), 171–187.

CALVETE, D., DODD, N., FALQUÉS, A. & VAN LEEUWEN, S. 2005. Morphological development of rip channel systems: Normal and near-normal wave incidence. *Journal of Geophysical Research: Oceans,* 110(C10).

CASTELLE, B., MARIEU, V., BUJAN, S., SPLINTER, K. D., ROBINET, A., SÉNÉCHAL, N. & FERREIRA, S. 2015. Impact of the winter 2013–2014 series of severe Western Europe storms on a double–barred sandy coast: beach and dune erosion and megacusp embayments. *Geomorphology,* 238, 135–148.

CLARKE, D. & ELIOT, I. 1988. Low-frequency changes of sediment volume on the beachface at Warilla Beach, New South Wales, 1975–1985. *Marine Geology,* 79(3-4), 189–211.

COHN, N., RUGGIERO, P., DE VRIES, S. & GARCÍA-MEDINA, G. 2017. Beach growth driven by intertidal sandbar welding. *Proceedings of Coastal Dynamics*, 199, 12–16.

DA FONTOURA KLEIN, A. H., BENEDET FILHO, L. & SCHUMACHER, D. H. 2002. Short-term beach rotation processes in distinct headland bay beach systems. *Journal of Coastal Research,* 18(3), 442–458.

DAIL, H. J., MERRIFIELD, M. A. & BEVIS, M. 2000. Steep beach morphology changes due to energetic wave forcing. *Marine Geology,* 162(2-4), 443–458.

DE ALEGRIA-ARZABURU, A. R. & MASSELINK, G. 2010. Storm response and beach rotation on a gravel beach, Slapton Sands, UK. *Marine Geology,* 278(1-4), 77–99.

HARLEY, M. D., TURNER, I. L., SHORT, A. D. & RANASINGHE, R. 2005. *Comparison of Video, RTK–GPS and Conventional Beach Survey Methods.* Australia Barton: Institution of Engineers.

HARLEY, M. D., TURNER, I. L., SHORT, A. D. & RANASINGHE, R. 2011a. Assessment and integration of conventional, RTK–GPS and image-derived beach survey methods for daily to decadal coastal monitoring. *Coastal Engineering,* 58(2), 194–205.

HARLEY, M. D., TURNER, I., SHORT, A. & RANASINGHE, R. 2011b. A re-evaluation of coastal embayment rotation: the dominance of cross-shore versus alongshore sediment transport processes, Collaroy–Narrabeen Beach, southeast Australia. *Journal of Geophysical Research: Earth Surface,* 116(F4), 4033.

HAXEL, J. H. & HOLMAN, R. A. 2004. The sediment response of a dissipative beach to variations in wave climate. *Marine Geology,* 206(1-4), 73–99.

KOMAR, P. D. 1976. *Beach processes and sedimentation*. New Jersey: Prentice-Hall.

KOMAR, P. D. & INMAN, D. L. 1970. Longshore sand transport on beaches. *Journal of Geophysical Research,* 75(30), 5914-5927.

LEE, D. T. & SCHACHTER, B. J. 1980. Two algorithms for constructing a Delaunay triangulation. *International Journal of Computer & Information Sciences,* 9(3), 219–242.

LONGUET-HIGGINS, M. S. 1970. Longshore currents generated by obliquely incident sea waves: 1. *Journal of Geophysical Research,* 75(33), 6778–6789.

MASSELINK, G., AUSTIN, M., SCOTT, T., POATE, T. & RUSSELL, P. 2014. Role of wave forcing, storms and NAO in outer bar dynamics on a high-energy, macrotidal beach. *Geomorphology,* 226, 76–93.

MASSELINK, G., KROON, A. & DAVIDSON-ARNOTT, R. 2006. Morphodynamics of intertidal bars in wave–dominated coastal settings – a review. *Geomorphology,* 73(1-2), 33–49.

MASSELINK, G. & PATTIARATCHI, C. 2001. Seasonal changes in beach morphology along the sheltered

coastline of Perth, Western Australia. *Marine Geology,* 172(3-4), 243–263.

MCCARROLL, R. J., BRANDER, R. W., TURNER, I. L. & VAN LEEUWEN, B. 2016. Shoreface storm morphodynamics and mega-rip evolution at an embayed beach: Bondi Beach, NSW, Australia. *Continental Shelf Research,* 116, 74–88.

MILLER, I. M., WARRICK, J. A. & MORGAN, C. 2011. Observations of coarse sediment movements on the mixed beach of the Elwha Delta, Washington. *Marine Geology,* 282(3-4), 201–214.

MORTON, R. A., LEACH, M. P., PAINE, J. G. & CARDOZA, M. A. 1993. Monitoring beach changes using GPS surveying techniques. *Journal of Coastal Research,* 9(3), 702–720.

NICHOLLS, R. J., WONG, P., BURKETT, V., CODIGNOTTO, J., HAY, J., MCLEAN, R., RAGOONADEN, S. & WOODROFFE, C. 2007. Coastal systems and low-lying areas. Climate Change 2007: Impacts, Adaptation and Vulnerability. *In:* PARRY, M. L., CANZIANI, O. F., PALUTIKOF, J. P., VAN DER LINDEN, P. J. & HANSON, C. E. (eds.). *Contribution of Working Group II to the Fourth Assessment Report of the Intergovernmental Panel on Climate Change.* Cambridge: Cambridge University Press, pp. 315-356.

OJEDA, E. & GUILLÉN, J. 2008. Shoreline dynamics and beach rotation of artificial embayed beaches. *Marine Geology,* 253(1-2), 51–62.

PARDO-PASCUAL, J., GARCÍA-ASENJO, L., PALOMAR-VÁZQUEZ, J. & GARRIGUES-TALENS, P. 2005. New methods and tools to analyze beach-dune system evolution using a Real–Time Kinematic Global Positioning System and Geographic Information Systems. *Journal of Coastal Research,* 49, 34–39.

PHINN, S. R. & HASTINGS, P. A. 1992. Southern oscillation influences on the wave climate of south-eastern Australia. *Journal of Coastal Research,* 8(3), 579–592.

RANASINGHE, R., MCLOUGHLIN, R., SHORT, A. & SYMONDS, G. 2004. The Southern Oscillation Index, wave climate, and beach rotation. *Marine Geology,* 204(3-4), 273–287.

ROBINET, A., CASTELLE, B., IDIER, D., HARLEY, M. & SPLINTER, K. 2020. Controls of local geology and cross-shore/longshore processes on embayed beach shoreline variability. *Marine Geology,* 422, 106118.

SHORT, A. D. & MASSELINK, G. 1999. Embayed and structurally controlled beaches. *Handbook of Beach and Shoreface Morphodynamics,* 1(999), 230–249.

SHORT, A. D. & TREMBANIS, A. C. 2004. Decadal scale patterns in beach oscillation and rotation Narrabeen Beach, Australia–time series, PCA and wavelet analysis. *Journal of Coastal Research,* 20(2), 523–532.

SHORT, A. D., TREMBANIS, A. C. & TURNER, I. L. 2001. Beach oscillation, rotation and the southern oscillation, Narrabeen beach, Australia. *Coastal Engineering 2000,* 2439–2452.

SHORT, A. D. & TRENAMAN, N. 1992. Wave climate of the Sydney region, an energetic and highly variable ocean wave regime. *Marine and Freshwater Research,* 43(4), 765–791.

STIVE, M. J., AARNINKHOF, S. G., HAMM, L., HANSON, H., LARSON, M., WIJNBERG, K. M., NICHOLLS, R. J. & CAPOBIANCO, M. 2002. Variability of shore and shoreline evolution. *Coastal Engineering,* 47(2), 211–235.

STIVE, M. J. & WIND, H. G. 1982. A study of radiation stress and set–up in the nearshore region. *Coastal Engineering,* 6(1), 1–25.

STOJANOVIC, T. & FARMER, C. 2013. The development of world oceans & coasts and concepts of sustainability. *Marine Policy,* 42, 157–165.

THEUERKAUF, E. J. & RODRIGUEZ, A. B. 2012. Impacts of transect location and variations in along-beach morphology on measuring volume change. *Journal of Coastal Research,* 28(3), 707–718.

THOMAS, T., PHILLIPS, M. & LOCK, G. 2015. An analysis of subaerial beach rotation and influences of environmental forcing adjacent to the proposed Swansea Bay Tidal Lagoon. *Applied Geography,* 62, 276–293.

THOMAS, T., PHILLIPS, M. & WILLIAMS, A. 2010. Mesoscale evolution of a headland bay: beach rotation processes. *Geomorphology,* 123(1-2), 129–141.

THOMAS, T., PHILLIPS, M., WILLIAMS, A. & JENKINS, R. 2011a. Medium timescale beach rotation; gale climate and offshore island influences. *Geomorphology,* 135(1-2), 97–107.

THOMAS, T., PHILLIPS, M., WILLIAMS, A. & JENKINS, R. 2011b. Short–term beach rotation, wave climate and the North Atlantic Oscillation (NAO). *Progress in Physical Geography,* 35(3), 333–352.

TURKI, I., MEDINA, R., GONZALEZ, M. & COCO, G. 2013. Natural variability of shoreline position: observations at three pocket beaches. *Marine Geology,* 338, 76–89.

VAN DE LAGEWEG, W., BRYAN, K. R., COCO, G. & RUESSINK, B. 2013. Observations of shoreline–sandbar coupling on an embayed beach. *Marine Geology,* 344, 101–114.

WERNETTE, P. & HOUSER, C. 2022. Evidence for geologic control of rip channels along Prince Edward Island, Canada. *Physical Geography,* 43(2), 145–162.

WRIGHT, L., CHAPPELL, J., THOM, B., BRADSHAW, M. & COWELL, P. 1979. Morphodynamics of reflective and dissipative beach and inshore systems: Southeastern Australia. *Marine Geology,* 32(1-2), 105–140.

WRIGHT, L. D. & SHORT, A. D. 1984. Morphodynamic variability of surf zones and beaches: a synthesis. *Marine Geology,* 56(1-4), 93–118.

YOU, Z. J. & LORD, D. 2008. Influence of the El Niño–Southern Oscillation on NSW Coastal Storm Severity. *Journal of Coastal Research,* 24(10024), 203–207.

## SUPPLEMENTARY MATERIAL



**Figure S1.** Location of Stanwell Park Beach, NSW: (a) Relative to Sydney and Australia (source Google Earth); (b) Planimetric view (source Google Earth on 31/10/2014); and (c) Looking South (photo taken on 22/20/2016).



**Figure S2.** Location of Port Kembla waverider buoy situated 26.5 km from Stanwell Park Beach and Darkes Forest rainfall station situated 6.3 km from Stanwell Park Beach (source Google Earth on 31/10/2014).